

AFRL-VA-WP-TP-2003-319

**LONGITUDINAL CONTROL AND
FOOTPRINT ANALYSIS FOR A
REUSABLE MILITARY LAUNCH
VEHICLE**

Anhtuan D. Ngo and William B. Blake



JULY 2003

Approved for public release; distribution is unlimited.

This material is declared a work of the U.S. Government and is not subject to copyright protection in the United States.

**AIR VEHICLES DIRECTORATE
AIR FORCE RESEARCH LABORATORY
AIR FORCE MATERIEL COMMAND
WRIGHT-PATTERSON AIR FORCE BASE, OH 45433-7542**

20030825 015

| REPORT DOCUMENTATION PAGE | | | | <i>Form Approved</i> OMB No. 0704-0188 | |
|---|------------------------------------|--|---|--|---|
| The public reporting burden for this collection of information is estimated to average 1 hour per response, including the time for reviewing instructions, searching existing data sources, gathering and maintaining the data needed, and completing and reviewing the collection of information. Send comments regarding this burden estimate or any other aspect of this collection of information, including suggestions for reducing this burden, to Department of Defense, Washington Headquarters Services, Directorate for Information Operations and Reports (0704-0188), 1215 Jefferson Davis Highway, Suite 1204, Arlington, VA 22202-4302. Respondents should be aware that notwithstanding any other provision of law, no person shall be subject to any penalty for failing to comply with a collection of information if it does not display a currently valid OMB control number. PLEASE DO NOT RETURN YOUR FORM TO THE ABOVE ADDRESS. | | | | | |
| 1. REPORT DATE (DD-MM-YY) July 2003 | | 2. REPORT TYPE Conference Paper Preprint | | 3. DATES COVERED (From - To) | |
| 4. TITLE AND SUBTITLE LONGITUDINAL CONTROL AND FOOTPRINT ANALYSIS FOR A REUSABLE MILITARY LAUNCH VEHICLE | | | | 5a. CONTRACT NUMBER In-house | |
| | | | | 5b. GRANT NUMBER | |
| | | | | 5c. PROGRAM ELEMENT NUMBER N/A | |
| | | | | 5d. PROJECT NUMBER N/A | |
| 6. AUTHOR(S) Anh Tuan D. Ngo and William B. Blake | | | | 5e. TASK NUMBER N/A | |
| | | | | 5f. WORK UNIT NUMBER N/A | |
| | | | | 8. PERFORMING ORGANIZATION REPORT NUMBER AFRL-VA-WP-TP-2003-319 | |
| 7. PERFORMING ORGANIZATION NAME(S) AND ADDRESS(ES) Control Theory Optimization Branch (AFRL/VACA) Control Sciences Division Air Vehicles Directorate Air Force Research Laboratory, Air Force Materiel Command Wright-Patterson Air Force Base, OH 45433-7542 | | | | 10. SPONSORING/MONITORING AGENCY ACRONYM(S) AFRL/VACA | |
| | | | | 11. SPONSORING/MONITORING AGENCY REPORT NUMBER(S) AFRL-VA-WP-TP-2003-319 | |
| 9. SPONSORING/MONITORING AGENCY NAME(S) AND ADDRESS(ES) Air Vehicles Directorate Air Force Research Laboratory Air Force Materiel Command Wright-Patterson Air Force Base, OH 45433-7542 | | | | | |
| 12. DISTRIBUTION/AVAILABILITY STATEMENT Approved for public release; distribution is unlimited. | | | | | |
| 13. SUPPLEMENTARY NOTES To be presented at the American Institute of Aeronautics & Astronautics - GNC, Denver, CO, August 11, 2003. This material is declared a work of the U.S. Government and is not subject to copyright protection in the United States. | | | | | |
| 14. ABSTRACT This paper examines two concepts for a reusable military launch system (RMLS). Both are rocket powered vertical takeoff-horizontal landing configurations. One is a conventional wing-body configuration like the Space Shuttle, and the other is a lifting body configuration. The lifting body design lands in an inverted attitude, which significantly reduces the maintenance requirements for the vehicle's thermal protection system. The longitudinal stability and control characteristics are examined, and footprint calculations are made for re-entry. | | | | | |
| 15. SUBJECT TERMS | | | | | |
| 16. SECURITY CLASSIFICATION OF: | | | 17. LIMITATION OF ABSTRACT: SAR | 18. NUMBER OF PAGES 16 | 19a. NAME OF RESPONSIBLE PERSON (Monitor) Anh Tuan D. Ngo 19b. TELEPHONE NUMBER (Include Area Code) (937) 255-8494 |
| a. REPORT Unclassified | b. ABSTRACT Unclassified | c. THIS PAGE Unclassified | | | |

Longitudinal Control and Footprint Analysis for a Reusable Military Launch Vehicle

Anhtuan D. Ngo and William B. Blake
Air Force Research Laboratory/VACA
2210 Eighth Street, Bldg 146
Wright-Patterson AFB, OH. 45433-7531

Email: anhtuan.ngo@va.af.mil/william.blake2@wpafb.af.mil

Abstract

This paper examines two concepts for a reusable military launch system (RMLS). Both are rocket powered vertical takeoff-horizontal landing configurations. One is a conventional wing-body configuration like the Space Shuttle, the other is a lifting body configuration. The lifting body design lands in an inverted attitude, which significantly reduces the maintenance requirements for the vehicle's thermal protection system. The longitudinal stability and control characteristics are examined, and footprint calculations are made for re-entry.

α : angle of attack
 β : sideslip angle
 γ : Flight path angle
 δ : Control deflection
 θ : Longitude
 μ : Gravitational parameter
 ρ : Air density
 σ : Bank angle
 ϕ : Latitude
 ψ : Heading angle

Nomenclature

\bar{c} : Wing chord
 C_A : Axial force coefficient
 C_D : Drag coefficient
 C_{D_0} : Zero-lift drag coefficient
 C_L : Lift coefficient
 C_m : Pitching moment coefficient
 C_{m_0} : Pitching moment coef. with zero control deflection
 C_{m_δ} : Pitching moment coef. due to control deflection
 C_N : Normal force coefficient
 E : Specific Energy
 \tilde{g} : Effective gravitational constant
 h : Altitude
 J : Objective function
 k : Induced drag factor
 m : Mass of the vehicle
 M : Mach number
 R_o : Earth's radius
 S : Wing area
 v : Velocity
 W : Weight

1 Introduction

In recent years, the increasing potential of space in military and commercial applications has attracted interest in space operation vehicles by governments and industries. The renewed interest has resulted in various design studies and engineering development programs such as NASA's X-34 hypersonic rocket powered test vehicle, and X-37 reusable upper stage and satellite bus, X-33 program for demonstrating single-stage to orbit, the Ballistic Missile Defense Organization's Single-Stage Rocket Technology program that built the Delta Clipper-Experimental (DC-X) experimental reusable spaceplane. The objectives of these design studies and engineering programs are to advance the technologies required for affordable and reliable space flights such as composite propellant tanks, lightweight robust airframe, long life-time thermal protection system. Furthermore, to make space access more routine, NASA's Space Launch Initiative (SLI) aims to develop a second generation reusable launch vehicle that reduces cost while improving safety and reliability. Parallel to NASA's effort in meeting requirements of reusable launch vehicles for civilian applications is the Department of Defense's National Aerospace Initiative (NAI) which seeks to meet the unique requirements

of military space operation vehicles such as launch-on-demand along with affordability, safety, and reliability. As a result, increasing focus is placed on technologies that enable the space vehicles to have aircraft-like characteristics such as safety, operability, supportability, turn-around-time, and affordability. Supporting this space effort to meet the goals of future military space operation vehicles, preliminary design studies are underway at the Air Force Research Laboratory. This paper will examine the longitudinal stability and re-entry footprint for two of these designs. Both include technologies intended to improve vehicle operability and significantly reduce launch turnaround times.

2 Longitudinal Stability Prediction

Missile Datcom (Ref. [1]) was used to calculate the longitudinal aerodynamic characteristics of the vehicle. Missile Datcom is a widely used engineering-level code that uses the component buildup technique to predict vehicle aerodynamics. Code input consists of body, wing and tail geometry, Mach number, altitude, angle of attack and control deflections. Control devices are limited to either all moving controls or plain trailing edge flaps. At each flight condition the six-body axis force and moment coefficients are provided. Both theoretical and empirical methods are included that encompass the entire speed regime from subsonic to hypersonic. An improved method for calculating the center of pressure of a wing with a large strake (typical of many re-entry vehicles) was recently incorporated (Ref [2]). Missile Datcom has been shown to provide very good agreement with experimental data for a variety of missile configurations (Ref. [3]). To validate the code for RLV type configurations, extensive comparisons have been made with wind tunnel data for the X-34 and X-40 configurations. Sample results for the X-34 shown in Fig 1 (Ref. [4]) will be given here. Lift coefficient is predicted very well at both transonic and hypersonic speeds, as indicated in Figure 2. The large reduction in lift curve slope at hypersonic speeds is evident. Pitching moment comparisons are shown in Figure 3. At hypersonic speeds, both the prediction and data show that the configuration is unstable at low angles of attack and becomes stable at the high angles of attack attained during re-entry. At transonic speeds, the configuration is very stable with an unstable break between 10 and 20 degrees. Although Missile Datcom correctly predicts the slope and the break, the zero angle of attack value is underpredicted. This is probably because the code ignores the effect of forebody camber. The overall shift in static stability represents a center of pressure travel of about 6 percent of the body length.

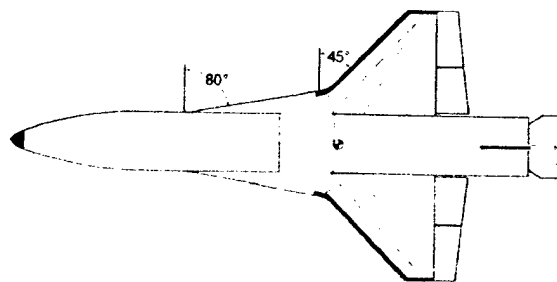


Figure 1: X-34 Reusable Launch Vehicle

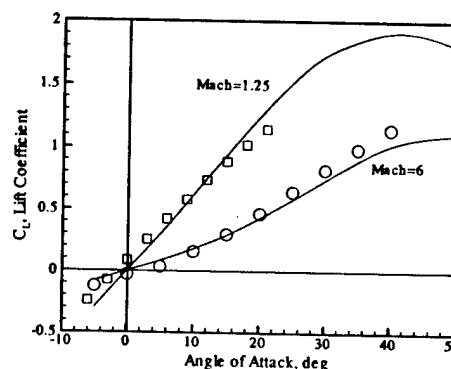


Figure 2: X-34 Lift Coefficient Comparison

3 Study Vehicles

Two USAF developed designs are the study vehicles for the present paper. Both designs are scaled versions of larger vehicles, and are intended to demonstrate technologies for rapid turnaround launch concepts. Both are rocket powered, vertical takeoff and horizontal landing concepts. One is a wing-body configuration, similar to the Space Shuttle (Ref. [5]) and X-34 (Ref. [4]), while the other is a lifting body similar to the X-24B (Ref. [6]). One unique feature of the lifting body concept is that it lands in an inverted attitude, with the thermal protection system on the top. The designs are shown in Figures 4, 5 and 6. The vehicles as modeled by Missile Datcom are shown in Figure 7, along with key dimensions.

The wing-body configuration is similar to the Space Shuttle except that the vertical tails are mounted on the wing tips. This would allow two such vehicles to be stacked one atop the other. The fuselage is 53 ft long with a fineness ratio of 5. The relatively low fineness ratio enhances accessibility and operability while the vehicle is in a vertical attitude prior to launch. Over-

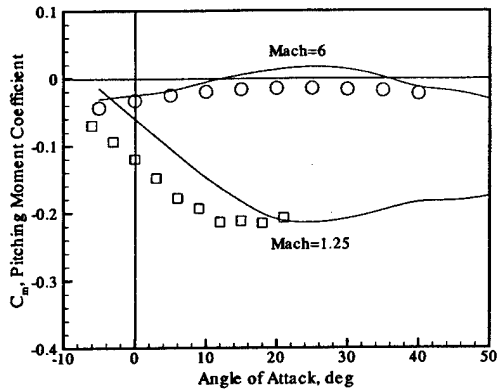


Figure 3: X-34 Pitching Moment Coefficient Comparison

all, the vehicle is 61 ft long with a wing span is 38.7 ft and wing area is 657.8 sq ft. The vehicle empty weight (for re-entry) is 49,340 lb, which gives a wing loading of about 75 lb/sq ft. The vehicle has five control effectors, an elevon on each wing, a body flap below the rocket nozzle, and rudders on the wing-tip mounted vertical tails. The tip mounted tails end-plate the wing at subsonic speeds, increasing lift and decreasing landing speed. The center of gravity of the vehicle is 38 ft from the nose, or 0.72 of the body length.

One of the major maintenance items on the Space Shuttle is the thermal protection system (TPS) on the bottom of the vehicle. The tiles and seals that compose the TPS must be laboriously inspected and replaced in many cases after each mission. One major problem is the seals around the landing gear doors. Placing the landing gear on the top of the vehicle, and inverting the vehicle prior to landing, would remove the need for these seals, reducing TPS maintenance requirements. An inverted landing configuration would also have much greater accessibility to the engines, payload, systems, and fuel tanks. These considerations led to the design of an inverted landing configuration. To simplify the landing gear integration, a lifting body concept was selected instead of a wing-body concept. It was scaled to have the same re-entry weight as the conventional design. The body length is 80.3 ft with a width of 30.2 ft. Side mounted vertical tails, which are canted outboard 10 degrees, are mounted forward of the body base. The vehicle planform area is 1575 sq ft. This results in a wing loading of 31 lb/sq ft, much lower than the wing-body design. The vehicle has four control devices, two rudders and two elevons, which are mounted aft of the body. The center of gravity of the

vehicle is 49.8 ft from the nose, or 0.62 of the body length.

Inverted landing designs are not new, they were studied during the X-30 NASP program to address inlet integration issues. An inverted landing design can also improve landing performance by reducing landing speeds. Inverting the vehicle changes the body camber from nose down to nose up during landing. The control deflection required to trim this camber change increases lift, which decreases landing speed. This increment will be reduced by ground effects, since inverting the vehicle moves the wing away from the ground. Calculations indicate landing speeds reductions of 10 Kts can be attained. This would help reduce maintenance on tires and brakes, another problem for the Space Shuttle.



Figure 4: Wing-Body Configuration - Side View

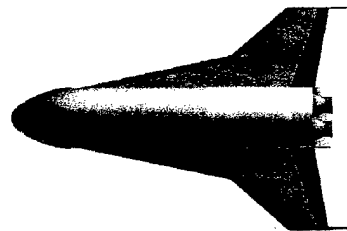


Figure 5: Wing-Body Configuration - Top View

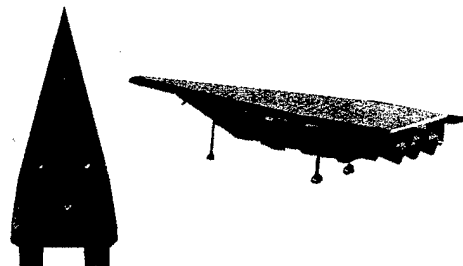


Figure 6: Lifting-Body Configuration

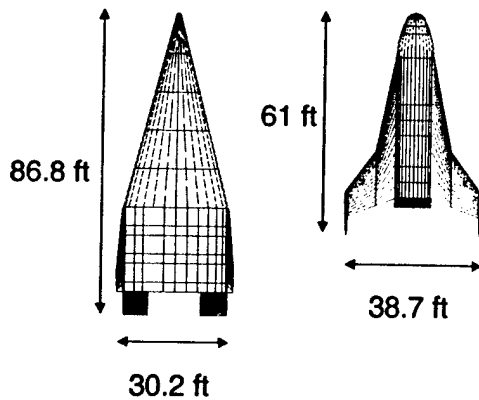


Figure 7: Missile Datcom Geometries

4 Longitudinal Aerodynamics

Predicted lift (L), drag (D), and lift to drag ratio (L/D) characteristics of the wing-body configuration at subsonic, transonic and hypersonic speeds are shown in Figures 8 through 11. The lift and drag characteristics are similar to both the Space Shuttle (Ref. [5]) and X-34 (Ref. [4]), with lift curve slope of about 4/radian at low speeds which decreases significantly at hypersonic speeds. The angle of attack for maximum lift increases with increasing Mach number, from 30 degrees at Mach 0.3 to 50 degrees at Mach 20. The maximum L/D decreases from about 4.5 at subsonic speeds to just under 2 at hypersonic speeds. At hypersonic speeds, the typical flight angle of attack (≈ 30 deg) is much higher than the predicted angle of attack for maximum L/D .

Lift, drag and L/D characteristics for the lifting body configuration are shown in Figures 12 through 15. The lift and drag characteristics are similar to the X-24B (Ref. [6]), with a lift curve slope of just less than 2/radian at low speeds which does not change significantly at transonic or hypersonic speeds. There is no sharp stall at subsonic speeds, in contrast to the conventional configuration. The angle of attack for maximum lift does not change significantly with speed. The maximum L/D at subsonic speeds is about 3.5, more than 20% lower than the conventional configuration. At hypersonic speeds, however, maximum L/D is much higher than for the wing-body configuration. This is typical for this type of configuration.

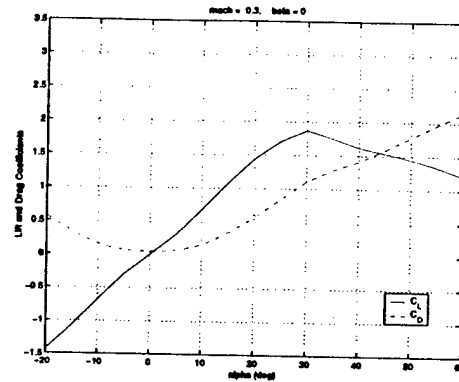


Figure 8: Wing-Body Lift and Drag Coef. at Mach 0.3

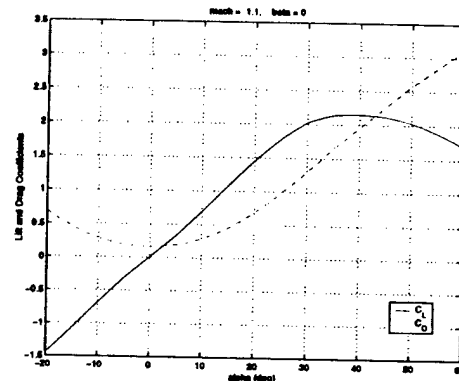


Figure 9: Wing-Body Lift and Drag Coef. at Mach 1.1

5 Longitudinal Stability and Control

The ability of the vehicle to maintain its longitudinal equilibrium is required before any maneuver is performed by the vehicle. It is therefore of interest to examine the ability of the control surfaces of the vehicle to zero out the wing-body pitching moment so that the equilibrium equations is satisfied:

$$M_o(\alpha, \beta, M) + M_\delta(\alpha, \beta, M) = 0 \quad (1)$$

We note that in Equation 1, the wing-body pitching moment M_o and total control effector pitching moment M_δ can be written as

$$M_o = \frac{1}{2} \rho v^2 \bar{c} S C_{M_o}$$

$$M_\delta = \frac{1}{2} \rho v^2 \bar{c} S C_{M_\delta}$$

where ρ is the air density, v is the velocity, S is the plane form area, \bar{c} is the mean aerodynamic chord, C_{M_o} is the wing-body pitching coefficient, C_{M_δ} is the total control pitching coefficient. The control pitching coefficient can be further expressed as

$$C_{M_\delta} = C_{M_{\delta_1}} + \dots + C_{M_{\delta_m}}$$

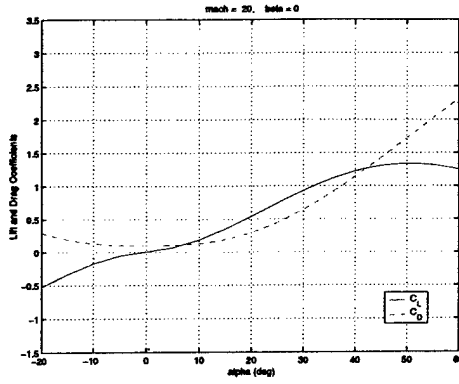


Figure 10: Wing-Body Lift and Drag Coef. at Mach 20

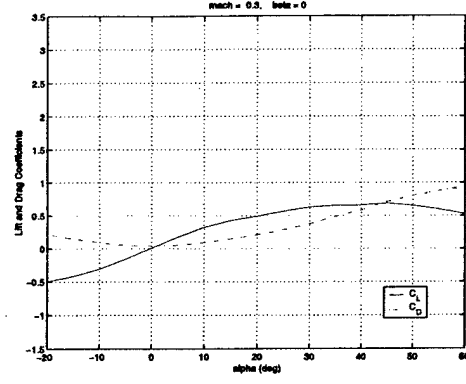


Figure 12: Lifting-Body Lift and Drag Coef. at Mach 0.3

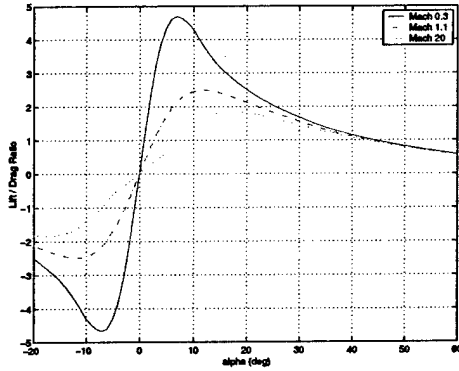


Figure 11: Wing-Body $\frac{L}{D}$ at Mach 0.3, 1.1, 20

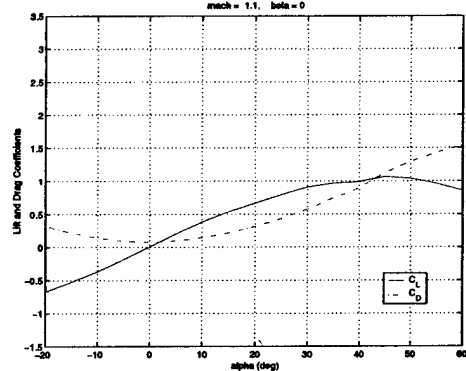


Figure 13: Lifting-Body Lift and Drag Coef. at Mach 1.1

The upper bound \overline{C}_{M_δ} and lower bound \underline{C}_{M_δ} of C_{M_δ} can be expressed as

$$\begin{aligned}\overline{C}_{M_\delta} &= \overline{C}_{M_{\delta_1}} + \dots + \overline{C}_{M_{\delta_m}} \\ \underline{C}_{M_\delta} &= \underline{C}_{M_{\delta_1}} + \dots + \underline{C}_{M_{\delta_m}}\end{aligned}$$

where over the range of each control effector δ_i , e.i. $\underline{\delta}_i \leq \delta_i \leq \overline{\delta}_i$, we have

$$\begin{aligned}\overline{C}_{M_{\delta_i}} &= \max_{\delta_i} C_m(\delta_i) \\ \underline{C}_{M_{\delta_i}} &= \min_{\delta_i} C_m(\delta_i)\end{aligned}$$

Thus at a given sideslip angle β , and Mach number M , and an angle of attack α , the flight condition is trimmable if

$$\begin{aligned}C_{M_o}(\alpha, \beta, M) + \overline{C}_{M_\delta}(\alpha, \beta, M) &\geq 0 \\ \text{and} \\ C_{M_o}(\alpha, \beta, M) + \underline{C}_{M_\delta}(\alpha, \beta, M) &\leq 0\end{aligned}\quad (2)$$

Figures 16, 17, and 18 show the pitching moment coefficient for the wing-body configuration C_{M_o} along with residual pitching moment's upper bound ($C_{M_o} + \overline{C}_{M_\delta}$) and lower bound ($C_{M_o} + \underline{C}_{M_\delta}$) at zero sideslip, i.e.

$\beta = 0$, over a range of angles of attack α for different Mach numbers. These figures show that the vehicle is statically unstable at low angles of attack at both subsonic and hypersonic speeds, and stable at transonic speeds. At Mach=0.3, the amount of instability at low speeds is low and should be easily accommodated by a flight control system. For a dynamic pressure of 300 psf, unlikely to be exceeded during approach, the time to double amplitude of the pitch instability is about 0.9 sec. The vehicle is untrimmable above 20 degrees angle of attack subsonically. At Mach=1.1, the vehicle is trimmable to angles of attack of almost 40 degrees, although there is a pitchup at 20 degrees angle of attack. At Mach=20, there is a stable break in the pitching moment curve at about 25 degrees angle of attack. This shows that the vehicle would be stable for a typical re-entry (AOA 30 deg). Both the X-34 (Ref. [4]) and Space Shuttle (Ref. [5]) have a similar characteristic. The vehicle is also trimmable at all angles of attack hypersonically.

The pitching moment characteristics of the lifting-body configuration are shown in Figures 19, 20, and 21. At low angles of attack, the vehicle is stable at subsonic and transonic speeds, and unstable at hypersonic speeds. Beyond 10 degrees angle of attack, there is a

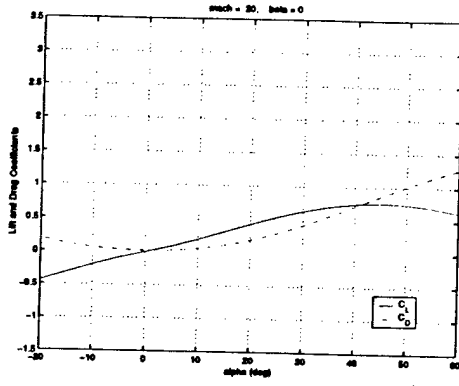


Figure 14: Lifting-Body Lift and Drag Coef. at Mach 20

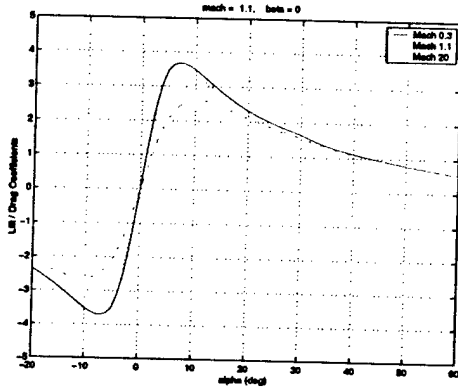


Figure 15: Lifting-Body $\frac{L}{D}$ at Mach 0.3, 1.1, 20

slight pitchup at subsonic and transonic speeds. The vehicle is trimmable up to 40 degrees angle of attack at both $M = 0.3$ and $M = 1.1$. It is also trimmable at all negative angles of attack at these speeds. This gives a wide range of flight conditions where the vehicle is capable of performing the 180 degree roll maneuver so it can land inverted. At $M = 20$, there is a stable break in the pitching moment at about 15 degrees angle of attack. This shows that, like the conventional configuration, the vehicle would be stable for a typical re-entry. The vehicle is also trimmable at all angles of attack hypersonically.

6 Footprint Calculation

The vehicle is assumed to be stabilized with an inner loop attitude controller, the dynamic equations for the un-powered vehicle over a non-rotating earth can be written as:

$$\dot{h} = v \sin(\gamma) \quad (3)$$

$$\dot{\theta} = \frac{v \cos(\gamma) \cos(\psi)}{(R_o + h)} \quad (4)$$

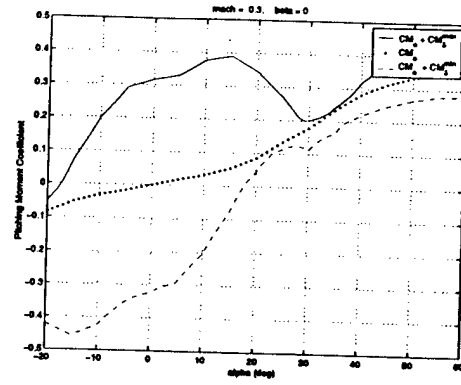


Figure 16: Wing-Body Pitching Moment Coef. at Mach 0.3

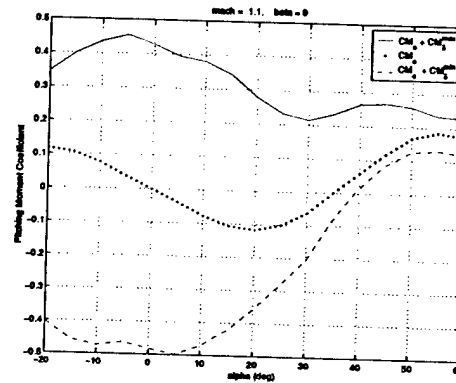


Figure 17: Wing-Body Pitching Moment Coef. at Mach 1.1

$$\dot{\phi} = \frac{v \cos(\gamma) \sin(\psi)}{(R_o + h)} \quad (5)$$

$$\dot{v} = \frac{-D}{m} - \frac{\mu \sin(\gamma)}{(R_o + h)^2} \quad (6)$$

$$\dot{\gamma} = \frac{L \cos(\sigma)}{mv} - \frac{\mu \cos(\gamma)}{v(R_o + h)^2} + \frac{v \cos(\gamma)}{(R_o + h)} \quad (7)$$

$$\dot{\psi} = \frac{L \sin(\sigma)}{mv \cos(\gamma)} - \frac{v \cos(\gamma) \cos(\psi) \tan(\phi)}{(R_o + h)} \quad (8)$$

Figure 22 illustrates the coordinate system used to model the vehicle.

Induced aerodynamic drag and friction acting on the vehicle cause the total energy of the un-powered vehicle to be monotonically decreasing. The vehicle footprint then consists of points on the earth's surface at which the total energy decreases to a set value. When its energy reaches this value, the vehicle then enters the final part of its trajectory called terminal area energy management phase. Combining its velocity v and altitude h in an energy-state approximation (Ref. [7]), a reduced order model can be obtained to simplify the vehicle description. The specific energy of the vehicle

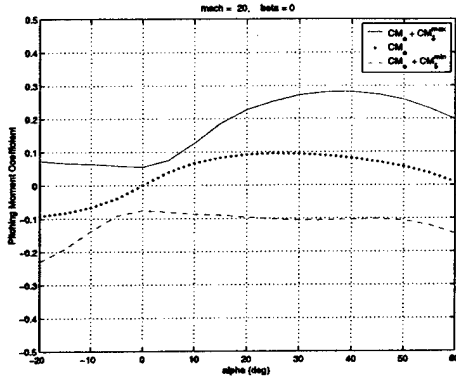


Figure 18: Wing-Body Pitching Moment Coef. at Mach 20

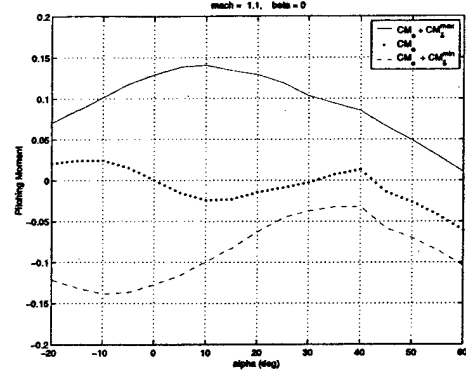


Figure 20: Lifting-Body Pitching Moment Coef. at Mach 1.1

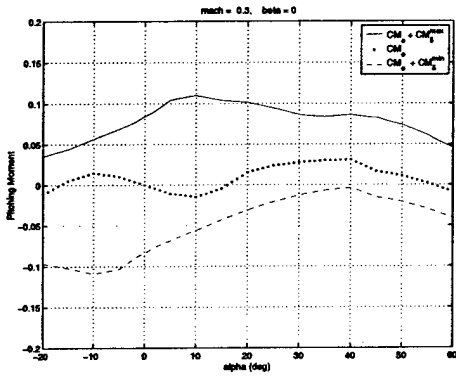


Figure 19: Lifting-Body Pitching Moment Coef. at Mach 0.3

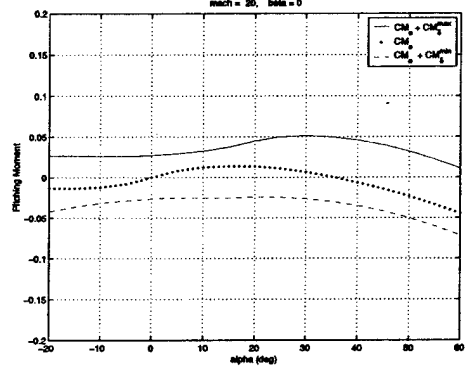


Figure 21: Lifting-Body Pitching Moment Coef. at Mach 20

can be expressed as

$$E = \frac{1}{2}v^2 + \frac{\mu}{(R_o + h)^2}h \quad (9)$$

From equations 3, 6, and 9, the rate of decrease in the vehicle's energy is

$$\frac{dE}{dt} = -\frac{vD}{m} - \frac{2\mu hv \sin(\gamma)}{(R_o + h)^3} < 0 \quad (10)$$

Assuming that the vertical forces acting on the vehicles are in equilibrium and its vertical motion frequency dynamics are much faster its horizontal motion dynamics, the flight path angle can be taken to be near zero, i.e., $\gamma \approx 0$. Moreover, since the acceleration normal to the velocity vector is small, i.e., $(v\dot{\gamma} \approx 0)$ and $v \neq 0$, the time-rate of change of the flight path angle can then be taken to be essentially zero, i.e., $\dot{\gamma} \approx 0$. From equation 7, we have

$$L = \frac{m}{\cos(\sigma)} \left(\frac{\mu}{(R_o + h)^2} - \frac{v^2}{(R_o + h)} \right) \quad (11)$$

With

$$L = \frac{1}{2}\rho v^2 S C_L \quad (12)$$

$$D = \frac{1}{2}\rho v^2 S C_D, \text{ and } C_D = C_{D_o} + kC_L^2 \quad (13)$$

we can combine equations 11 and 12 into equation 13 to get

$$D = \frac{1}{2}\rho v^2 S C_{D_o} + \frac{2m^2 k \bar{g}^2}{\rho v^2 \cos^2 \sigma} \quad (14)$$

where \bar{g} is the effective gravity constant:

$$\bar{g} = \frac{\mu}{R_o + h} - \frac{v^2}{R_o + h}$$

Given the initial velocity $v(t_o) = v_o$, and initial altitude $h(t_o) = h_o$, the vehicle specific energy $E(t)$ can

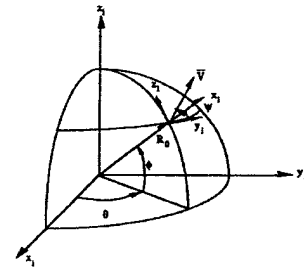


Figure 22: Coordinates System

be calculated according equation 10:

$$E(t) = E_o + dE = \frac{1}{2}v_o^2 + \frac{\mu h_o}{(R_o + h)^2} + dE \quad (15)$$

The vehicle's velocity $v(t)$ can be derived from the current specific energy $E(t)$:

$$v(t) = \sqrt{2E(t) - \frac{\mu h}{(R_o + h)^2}} \approx \sqrt{2E(t)} \quad (16)$$

since the vehicle flight altitude h is small when compared to the earth's radius R_o . From the above discussion, the unpowered vehicle under energy-state approximations has the reduced-order model $\dot{x} = f(x, u, t)$ of the form:

$$\dot{\theta} = \frac{v \cos(\psi)}{(R_o + h) \cos(\phi)} \quad (17)$$

$$\dot{\phi} = \frac{v \sin(\psi)}{R_o + h} \quad (18)$$

$$\dot{\psi} = \frac{z\bar{g}}{v} - \frac{v \cos(\psi) \tan(\phi)}{R_o + h} \quad (19)$$

$$\dot{E} = \frac{-Dv}{m} \quad (20)$$

where $x = [\theta, \phi, \psi, E]^T$ is the vehicle state vector. The control inputs $u = [\rho, z]^T$ are the air density, $\rho = \rho(h)$, and the tangent of the bank angle, $z = \tan(\sigma)$. The optimization objective is to find the control vector $u = [\rho, z]$ such that, at time $t = t_f$, the crossrange position specified by the vehicle latitude $\phi(t_f)$ is maximized for a given downrange value $\theta_f = \theta(t_f)$:

$$\max_{\rho, z} J = \int_{t_o}^{t_f} -\dot{\phi} dt \quad (21)$$

The initial values of the vehicle states are taken to be $\theta(t_o) = 0$, $\phi(t_o) = 0$, $\psi(t_o) = 0$ and $E(t_o) = E_o$. Following a similar derivation for the optimal control vector z as shown in (Ref. [8]), we have

$$\rho_{opt} = \sqrt{\frac{4m^2 k \bar{g}^2 (1 + z^2)}{v^2 SC_{do}}} \quad (22)$$

The optimum bank angle σ associated with $z = \tan(\sigma)$ is

$$z_{opt} = \frac{\cos(\phi) \sin(\bar{\theta}) (\frac{\mu}{R^2} - \frac{v^2}{R}) \frac{R}{v^2}}{\cos(\bar{\theta}) \sin(\psi) - \sin(\phi) \sin(\bar{\theta}) \cos(\psi)} \quad (23)$$

$$\tan(\theta_f) = \tan(\theta'_f) \cos(\psi'_o) + \frac{\tan(\phi'_f) \sin(\psi'_f)}{\cos(\theta'_f)}$$

$$\sin(\phi_f) = \sin(\phi'_f) \cos(\psi'_o) - \sin(\theta'_f) \cos(\phi'_f) \sin(\psi'_f)$$

Equations 22 and 23 give the optimal cross-range $\phi(t_f)$ for a given downrange θ_f . Iterations on the initial values of θ_f may be necessary so that the initial guess matches the final value $\theta(t_f)$ resulted from the equations 20.

7 Footprint Results

In this section, we apply the method for the footprint calculation to the study vehicles. At the beginning of the reentry phase, the 1534-slug vehicle attains the velocity of 12,500 feet/second at an altitude of 210,000 feet. With this initial energy, the unpowered vehicle's crossrange is calculated until its final energy is equivalent to the energy at the final speed of 1500 feet/second and 60,000 feet of altitude. This corresponds to 0.03 of the initial energy.

An important requirement that must be satisfied in calculating the vehicle footprint is the maintenance of lift to effective-weight equilibrium ($L=W$) while banking the vehicle:

$$L = \frac{1}{2} \rho v^2 SC_L = W = \frac{m\bar{g}}{\cos(\sigma)} \quad (24)$$

The respective normal and axial force coefficients C_N and C_A obtained from the vehicle's aerodynamic table are transformed into the corresponding lift and drag coefficients C_L and C_D :

$$C_L = \cos(\alpha) C_N - \sin(\alpha) C_A$$

$$C_D = \sin(\alpha) C_N + \cos(\alpha) C_A$$

A root solver based on the Secant method is then used to minimize the residual of $L - W$. Scanning the altitude that is 20,000 feet above and below the vehicle's current altitude, we look for the next optimal altitude command that minimizes the vehicle's drag subject to the constraint $L = W$. In addition to ensuring that the lift on the vehicle equals its weight, rotational equilibrium must also be enforced to maintain the vehicle's attitude. A trim routine is used to find the aero-control positions that are necessary to balance the base pitching moment produced by the wing-body portion of the vehicle. The lateral directional moments resulting from the wing-body portion of the vehicle are assumed to be zero (i.e. an assumption of zero steady-state sideslip and wing-body symmetry). In the trim routine, the roll, pitch and yaw control effectiveness of each aero-control surface at a fixed Mach number and angle of attack is found from the aerodynamic table using small perturbations. With B being the pitch control effectiveness matrix, δ the aero-control deflections and M_o the base pitching moment, a linear programming formulation (Ref. [9]) is used to find δ such that:

$$\min_{\delta} J = \|B\delta - M_o\|_1 \quad (25)$$

$$\text{subject to } \underline{\delta} \leq \delta \leq \bar{\delta}$$

The re-entry corridor is subjected to additional constraints on dynamic pressure and temperature. The maximum dynamic pressure is a structural constraint

and is limited to 2000 lb/sq ft. The maximum allowable temperature is a thermal constraint and is limited to 3600 deg R.

As discussed earlier, the footprint is sensitive to the specified final energy. Footprint calculations were generated for the wing-body configuration with final energies of 0.03 and 0.05 of the initial energy. The result is shown in Figure 23. The final energy has only a minimal impact on the downrange distance and virtually no impact on the crossrange distance. For the lowest energy case, the closest initial landing spot is 6 degrees longitude downrange of the re-entry point. The downrange footprint is about 14 degrees in longitude with a crossrange of ± 7 degrees in latitude. Note that these results are representative of an Equatorial landing. For landings at non-zero latitudes, the footprint becomes asymmetric.

The equations for the drag and subsequent energy loss (14, 20) can be expanded to give the following:

$$\dot{E} = -\frac{Dv}{m} = \frac{\tilde{g}C_{D_0}v^3}{2(W/S)} + \frac{2k\tilde{g}(W/S)}{\rho v \cos^2 \sigma}$$

Here, there are only three variables that are functions of the vehicle geometry, the zero lift drag coefficient (C_D), the induced drag factor (k) and the wing loading (W/S). This indicates that if a vehicle is scaled to another size and the wing loading is kept constant, then the resultant footprint will be identical. This was verified by calculating the footprint of a 0.75 scale version of the wing-body configuration. Note that this assumes that the relative center of gravity of gravity position also remains unchanged, so the trim characteristics of the scaled vehicles is the same.

The footprint for the lifting body configuration is shown in Figure 24, along with the footprint for the wing-body configuration. The footprint of the lifting body concept is slightly larger than the wing-body concept, while the closest initial landing spot is almost twice as far downrange (11 vs 6 degrees longitude). This increase in downrange is due to the much higher L/D of the lifting body concept. The crossrange capability is the same for both vehicles. It is not larger for the lifting body because it had insufficient lift to attain the optimum bank angles required for high crossrange trajectories (24). For the cases analyzed, the wing-body configuration was never bank angle limited.

8 Conclusion

In this paper, we have examined the longitudinal stability, control and re-entry footprint for two reusable military launch vehicle concepts. One is a conventional wing-body design, the other is a lifting body design

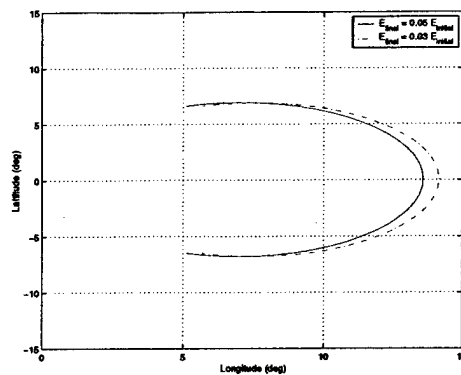


Figure 23: Wing-Body Configuration Footprint

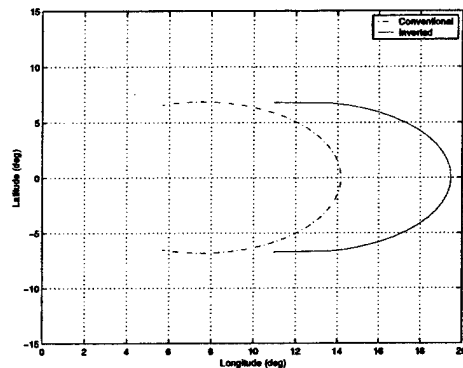


Figure 24: Footprints of Wing-Body & Lifting-Body Configurations

which lands in an inverted attitude. Inverted landing would significantly reduce the maintenance requirements on the thermal protection system. Both vehicles had similar stability characteristics although the lifting body concept had a wider range of trimmable angles of attack. Both vehicles had similar footprints in terms of overall size. However, the footprint of the lifting body configuration was further downrange because of its higher lift to drag ratio.

9 Acknowledgement

The authors wish to thank Alicia Hartong, Air Force Aeronautical Systems Center, and Gregory Moster, Air Force Research Laboratory, for providing the design data for the wing-body and lifting-body configurations.

References

- [1] Blake, W.B., "Missile Datcom User's Manual - 1997 Fortran 90 Revision," AFRL-VA-WP-TR-1998-3007, March 1998.
- [2] Blackmar, S., Miller, M., and Blake, W., "Ap-

proximate Methods for Center of Pressure Prediction of Multi-Segment Wings" *Proceedings of the 2003 Applied Aerodynamics Conference*, AIAA 2003-3934, June 2003.

[3] Packard, J, and Miller, M., "Assessment of Engineering Level Codes for Missile Aerodynamic Design and Analysis" *Proceedings of the 2000 Atmospheric Flight Mechanics Conference*, AIAA 2000-4590, Aug. 2000.

[4] Brauckmann, G.J., "X-34 Vehicle Aerodynamic Characteristics" *Journal of Spacecraft and Rockets*, Vol. 36, No. 2., 1999, pp. 229-239.

[5] Young, J.C., et al, "The Aerodynamic Challenges of the Design and Development of the Space Shuttle Orbiter" NASA CP 2342 (Part 1), pp. 209-263, January 1985.

[6] Nagy, C.J., and Kirsten, P.W., "Handling Qualities and Stability Derivatives of the X-24B Research Aircraft," AFFTC-TR-76-8, March 1976.

[7] E. S. Rutowski, "Energy Approach to the General Aircraft Performance Problem," *Journal of Aeronautical Sciences* Vol. 21, 1954, pp. 187-195.

[8] Ngo, A. D., Doman D.B, "Footprint Calculation Methods for a Reusable Launch Vehicle," ACC02-AIAA1032, American Control Conference (ACC-2002), Anchorage, Alaska, May 2002

[9] D. B. Doman, A. D. Ngo, D. B. Leggett, M. A. Saliers, "Development of A Hybrid Direct-Indirect Adaptive Control System for the X-33," in *Proceedings of the 2001 Guidance, Navigation and Control Conference*, AIAA 2001-4156, Aug. 2001.